

# Electron density measurement in a rf helium plasma by laser-collision induced fluorescence method

K. Dzierżęga,<sup>a)</sup> K. Musioł,<sup>a)</sup> E. C. Benck, and J. R. Roberts  
National Institute of Standards and Technology, Gaithersburg, Maryland 20899

(Received 12 March 1996; accepted for publication 6 June 1996)

Laser-collision induced fluorescence (LCIF) is the emission of light from states that have been populated by laser excitation and a subsequent collision. By simultaneously measuring the LCIF from two different states, it is possible to determine both the electron density and temperature of the low energy bulk electrons within a plasma. This method is described in detail and has been applied in the determination of the total, temporally averaged, and spatially resolved electron density in a rf (13.56 MHz) helium discharge in the Gaseous Electronics Conference reference cell. The rf discharge was operated at pressures  $P=33.3\text{--}133.3$  Pa (0.25–1.0 Torr) and peak-to-peak voltages of  $V_{pp}=75\text{--}300$  V were applied. We found the total electron density varied from  $1.8\times 10^8\text{ cm}^{-3}$  at  $P=33.3$  Pa and  $V_{pp}=75$  V to  $4.0\times 10^{10}\text{ cm}^{-3}$  at  $P=133.3$  Pa and  $V_{pp}=300$  V. A comparison of results from different experiments has been made. © 1996 American Institute of Physics. [S0021-8979(96)02818-6]

## INTRODUCTION

Recent developments in rf plasma-aided manufacturing have shown a great interest in rf plasma modeling and in the limitations of the plasma diagnostic tools presently used. There is a demand for alternative and complimentary diagnostic methods to get reliable results to fully understand plasma processes.

Among the many methods for rf plasma diagnostics, the Langmuir probe (LP) and microwave interferometer (MWI) are well established and have been commonly used for many years.<sup>1–7</sup> Temporally resolved electron densities,  $n_e$ , can be obtained with both methods but only the LP yields good spatial resolution and enables one to measure the electron energy distribution function (EEDF) as well. But because the electric probe is immersed in the plasma, the plasma can be perturbed making the results unreliable. Electron density can change, not only in the vicinity of the electric probe, but even globally. Thus, measured current–voltage ( $I\text{--}V$ ) characteristics can be easily misinterpreted. This is due to effects such as ionization near the probe, expansion of the probe sheath, probe contamination or probe circuit impedance, and influence of the rf field. Experimental requirements for the applicability of the LP method are often difficult to fulfill especially in discharges at higher pressures where the electron mean-free-path and ionization length become smaller than dimensions of the probe.

The nonintrusive MWI method, which is reasonably easy to perform, however, requires the knowledge of the shape of the electron density spatial distribution in order to determine the value of  $n_e$  at the center of the discharge due to the large spatial extent of the method. This fact makes the application of this method limited to axially symmetric medium.

The comparisons of these two methods<sup>6</sup> indicate that the results obtained agree well in a dc discharge. In rf discharges agreement within  $\pm 30\%$  has been reached at pressures

$P\leq 13.3$  Pa while at higher pressures the disagreement exceeds a factor of 2.

We have applied a nonintrusive method, called the laser collision-induced fluorescence (LCIF) method, as an alternative for measuring electron density with high spatial resolution in helium rf discharges in the Gaseous Electronics Conference (GEC) reference reactor. Laser-induced fluorescence (LIF) methods have been used as a tool to diagnose plasmas for many years. Dubreuil and Prigent<sup>8</sup> calculated  $n_e$  measuring the quenching coefficient of the LIF signal in a glow discharge. Tsuchida *et al.*<sup>9</sup> used the LIF to measure the spatial distribution of  $n_e$  assuming electron temperature  $T_e$  as a known parameter. Den Hartog *et al.*<sup>10</sup> determined both  $n_e$  and  $T_e$  from the LCIF in combination with kinetic equations for metastable levels in helium.

In this article we discuss the theoretical principles of the LCIF method as it applies to our rf plasma. The experimental setup is described and the results obtained are compared with other measurements of the electron density in GEC reference cells.

## PRINCIPLES OF THE METHOD

When atoms in a plasma are excited by the absorption of laser light, some lose their excitation energy directly as radiation, which is known as laser-induced fluorescence. Some of the excited atoms make transitions to higher lying states by collisions with plasma particles and then radiate, which we call laser collision-induced fluorescence. We introduce the intensity ratio  $F=I_C/I_L$  where  $I_C$  and  $I_L$  are the intensities of the LCIF and the LIF, respectively. In the case where electron collisions are a dominant excitation mechanism in the plasma, the ratio  $F$  is a function of electron density and an averaged electron excitation cross section  $\bar{\sigma}=\langle\sigma(v_e)\rangle$ , where  $\sigma$ ,  $v_e$  and  $\langle\rangle$  stand, respectively, for the electron excitation cross section, electron velocity, and the average over the EEDF. For a Maxwellian EEDF, the average value is a function of mean electron temperature  $T_e$ ,  $\bar{\sigma}=\bar{\sigma}(T_e)$  and can be easily calculated. Thus, if the electron excitation cross

<sup>a)</sup>Permanent address: Jagiellonian University, ul. Reymonta 4, 30-059 Kraków, Poland.

sections are known, by measuring the ratios  $F$  for two different electron collision processes,  $n_e$  and  $T_e$  can be simultaneously determined.

The potential application of LCIF to the measurement of electron temperature and density is not restricted to helium. This technique can be applied to a variety of different atomic and molecular systems, if the electron energy dependence of the appropriate averaged electron excitation cross sections are known. Although the electron excitation cross sections are well known for excitations from the ground state or metastable states of many atoms, ions and molecules, the electron excitation between higher energy excited states is often not well known. This is probably the most serious limitation to the use of LCIF measurements in other atomic and molecular systems.

If the electron energy dependence of the electron excitation cross sections are known, several properties of the plasma must be considered in order to choose appropriate transitions for LCIF measurements. (1) The plasma needs to be optically thin at all observed optical transitions. This is of particular importance at the laser wavelength, since the initial state is generally a highly populated metastable or ground state atom. If the plasma is optically thick at this wavelength, significant amounts of resonantly scattered laser radiation would excite atoms outside of the laser beam, destroying the spatial resolution of the LCIF measurement. (2) The electron collision rates need to be small compared to the optical transition rate of the LIF signal. Otherwise the LIF signal cannot be used to account for spatial variations of the metastable or ground state atom excited by the laser and for variations in the laser intensity. (3) The contribution of ion collisions to the final state must be negligible compared to the electron excitations. Usually, the average ion energy is much less than the average electron energy. Therefore, this problem can often be avoided by choosing energy gaps between the state populated by the laser and those excited by electron collisions to be large compared to the average ion energy. On the other hand, the energy gaps cannot be large compared to the average electron energy or the resulting signals will be too small to measure due to the low number of high energy electrons. (4) The states being populated by electron excitation must have average electron excitation cross sections with different electron energy dependence in order to make an accurate determination of  $n_e$  and  $T_e$ .

### ELECTRON DENSITY AND TEMPERATURE DETERMINATION OF A rf HELIUM DISCHARGE USING THE LCIF METHOD

In our experiment helium atoms are excited to the  $4^3P$  state from the highly populated ( $\sim 10^{11}$ – $10^{12}$  cm $^{-3}$ )  $2^3S$  metastable state<sup>7</sup> by the absorption of a 318.7 nm laser photon (Fig. 1). The  $4^3D$  and  $5^3D$  states are subsequently populated from the  $4^3P$  state by collisions at collision transfer rates  $R_2$  and  $R_3$ , respectively. The LIF from the  $4^3P$  level and the LCIF from the  $4^3D$  and  $5^3D$  levels are observed at the wavelengths 318.7, 447.1, and 402.6 nm, respectively.

The short laser excitation (6 ns) produces an excess population  $N_1(0)$  in the state  $4^3P$  and the immediate decay is described by a single exponential

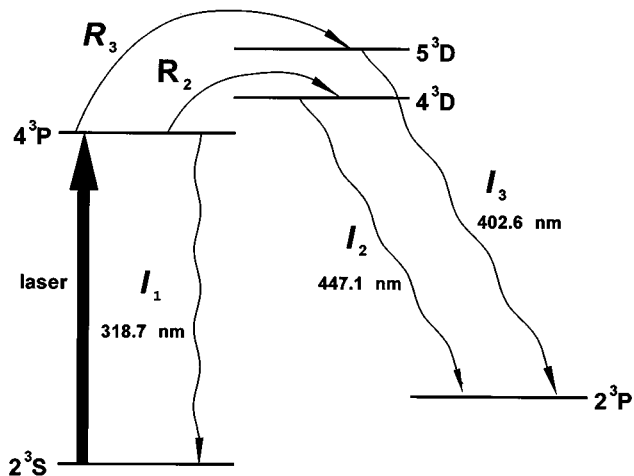


FIG. 1. The diagram of helium energy levels and collisional and radiative transition processes involved in LCIF.

$$N_1(t) = N_1(0)\exp(-t/\tau_1), \quad (1)$$

where  $\tau_1$  is the observed decay time including both collisional and radiative processes. Similarly, the population  $N_{2(3)}(t)$  of  $4^3D(5^3D)$  level can be described by the rate equation

$$dN_{2(3)}(t)/dt = -N_{2(3)}(t)/\tau_{2(3)} + R_{2(3)}N_1(t), \quad (2)$$

where  $\tau_{2(3)}$  is the observed decay time of the appropriate state. The first component on the right-hand side describes all depopulation processes, whereas the second component describes population from the lower state  $4^3P$  by collisions with the transfer rate  $R_{2(3)}$ . Substituting  $N_1(t)$  from Eq. (1) the solution for  $N_{2(3)}(t)$  is

$$N_{2(3)}(t) = \frac{R_{2(3)}N_1(0)}{1/\tau_{2(3)} - 1/\tau_1} [\exp(-t/\tau_1) - \exp(-t/\tau_{2(3)})]. \quad (3)$$

For an optically thin medium, the observed fluorescence intensity  $I_k(t)$  from level  $k$  is proportional to  $N_k(t)A_k\epsilon_k/\lambda_k$  where  $A_k$  is a corresponding radiative atomic transition probability,  $\epsilon_k$  is a relative quantum efficiency of a detection system and  $\lambda_k$  is a transition wavelength. The intensity ratio,  $F_{j1}$  of the time-integrated LCIF intensity to the time-integrated LIF intensity is

$$F_{j1} = \frac{\int_0^\infty I_j(t) dt}{\int_0^\infty I_1(t) dt} = \frac{R_j A_j \lambda_1 \epsilon_j}{A_1 \lambda_j \epsilon_1}, \quad j=2,3. \quad (4)$$

In the case of our low-pressure ( $P \leq 133.3$  Pa) and weakly ionized ( $[\text{He}^+] < 10^{-4} [\text{He}]$ ) plasma, collisions with electrons and atoms in a ground state play the dominant roles in population transfer between helium excited states. Hence, the collision transfer rate,  $R_j$  can be expressed as

$$R_j = R_j^{\text{at}} + R_j^{\text{el}}, \quad (5)$$

where  $R_j^{\text{at}}$  and  $R_j^{\text{el}}$  are the atom and electron collision transfer rates, respectively. The electron part is a product of electron density and electron temperature dependent average cross section for the electron collision excitation from state 1 to  $j$ ,

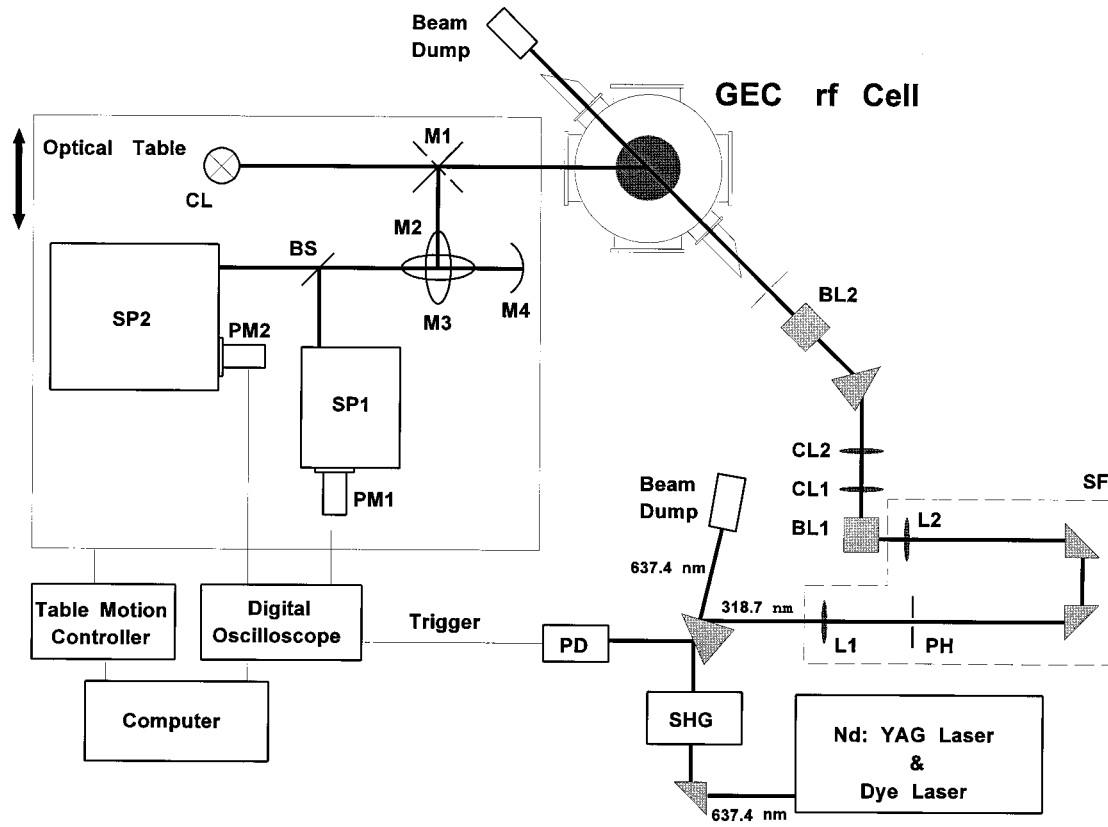


FIG. 2. Experimental setup: BL1 and BL2, beam lifts; BS, beam splitter; CL, calibration lamp; CL1 and CL2, cylindrical lenses; L1 and L2, spherical lenses; M1, M2, and M3, flat mirrors, M4, concave mirror; PD, photodiode; PH, pinhole; PM1 and PM2, photomultipliers; SF, spatial filter; SHG, second harmonic generator; SP1 and SP2, spectrometers.

$$R_j^{\text{el}} = n_e \bar{\sigma}_{1j}(T_e). \quad (6)$$

For two collisional processes as in Fig. 1, taking into account Eqs. (5) and (6), we can write

$$R_2^{\text{el}} = R_2 - R_2^{\text{at}} = n_e \bar{\sigma}_{12}(T_e), \quad (7)$$

$$R_3^{\text{el}} = R_3 - R_3^{\text{at}} = n_e \bar{\sigma}_{13}(T_e).$$

For a particular plasma condition,  $n_e$  and  $T_e$  can be numerically calculated from Eq. (7) using experimentally determined  $R_j^{\text{el}}$ .

## EXPERIMENTAL SETUP

The experimental arrangement is shown in Fig. 2. It consists of the laser system, the GEC rf cell and the detection system. A 30 Hz pulsed Nd:YAG-laser-pumped dye laser system with a frequency doubled output beam is used to obtain the required wavelength of 318.7 nm. The spatially uniform, 2 mm high and 7 mm wide 318.7 nm laser beam is formed using a spatial filter followed by two cylindrical lenses CL1 and CL2, and a diaphragm DP1. Its uniformity and dimensions have been checked with a CCD camera. The final energy of the 318.7 nm laser pulse is about 200  $\mu\text{J}$  with a spectral bandwidth less than  $0.1 \text{ cm}^{-1}$ . A system of right angle prisms and two beam lifts (BL1, BL2) are used to direct the laser beam into the interaction region of the rf discharge. The second beam lift, BL2 is placed in front of the

rf cell and the translation of its upper prism enables the laser to illuminate different plasma zones between the electrodes.

The rf plasma in helium is generated in the GEC rf reference cell.<sup>11,12</sup> Briefly, this cell is a rf discharge chamber equipped with two 10.2 cm diameter parallel-plate electrodes with a spacing of 2.5 cm. Gas is supplied to the plasma by a showerhead arrangement of small holes in the lower electrode. The flow of helium is maintained at  $1.7 \times 10^{-2} \text{ Pa m}^3/\text{s}$  (10 SCCM) and the pressures ranged from 33.3 to 133.3 Pa. The lower electrode is powered by a 13.56 MHz rf power supply, while the upper electrode is grounded. We apply peak-to-peak voltages,  $V_{\text{pp}}$  from 75 to 300 V. The powered electrode is aluminum and the grounded electrode is stainless steel in this experiment.

The LIF signals are observed at  $45^\circ$  with respect to the laser beam axis. The discharge is imaged onto the slits of two spectrometers SP1 and SP2 by the system of four mirrors M1 through M4. These mirrors act as a periscope, rotating the plasma image by  $90^\circ$ . Widths of the spectrometers' entrance and exit slits are set to  $250 \mu\text{m}$  to measure the total intensity of the spectral lines. The spatial resolution is 0.5 mm vertically and 7 mm horizontally. The spectrometer SP1 is set to monitor the LIF signal at 318.7 nm, while the SP2 is tuned to register the LCIF signal, either at 447.1 or 402.6 nm wavelength. The spectrometers are equipped with identical fast photomultipliers and are directly connected to a digital oscilloscope (350 MHz bandpass). The scope is externally

TABLE I. Measured quantities  $\tau_j$ ,  $R_j$  and  $R_j^{\text{at}}$  for collisional processes studied at different discharge pressures and  $V_{\text{pp}} = 300$  V. The radiative decay times are calculated to be 31.5 and 60.7 ns, respectively (see Ref. 12). The uncertainties are based on one standard deviation of up to six independent measurements.

$P$ (Pa)	$R_2^{\text{at}}$ ( $10^5 \text{ s}^{-1}$ )	$R_2$ ( $10^5 \text{ s}^{-1}$ )	$\tau_2$ (ns)	$\tau_3$ (ns)
133.3	$7.7 \pm 0.2$	$40.4 \pm 0.8$	$20.3 \pm 1.3$	$51 \pm 3$
66.6	$4.8 \pm 0.1$	$11.3 \pm 0.3$	$29.3 \pm 0.5$	$55 \pm 4$
33.3	$2.6 \pm 0.1$	$4.8 \pm 0.2$	$30.0 \pm 0.7$	$58 \pm 4$

triggered by a fast photodiode illuminated by the 318.7 nm laser beam reflected from the prism surface (Fig. 2).

The horizontal profiles of LIF signals are accomplished by translation of the optical table. The axial profiles are measured, first illuminating the appropriate plasma region with the laser beam and then translating the mirror M3 of the periscope to image the same region onto the spectrometers' slits. The spectral sensitivity of the experimental system is calibrated using a standard radiometric method with a tungsten ribbon lamp. The data acquisition system is operated and controlled by a computer.

## RESULTS

For a given plasma conditions and at a specific radial and axial position, LIF and LCIF signals are simultaneously collected into two channels of the oscilloscope and averaged over 1000 laser shots. Intensity ratios  $F_{j1}$  are obtained by integrating the signals over a time period of 400 ns. The total collision transfer rates are then determined from Eq. (4) utilizing atomic transition probabilities published by Wiese *et al.*<sup>13</sup> A two exponential fit is applied to the LCIF signals, according to Eq. (3), to determine the decay times  $\tau_2$  and  $\tau_3$ .

The atomic contribution  $R_j^{\text{at}}$  to the total collision transfer rate  $R_j$  is measured in a plasma sheath where there exists a negligible number of free electrons and where the concentration of atoms in the metastable state is much higher between the electrodes than outside their region so a better signal-to-noise ratio can be obtained.

Values of decay times, atomic, and total collision transfer rates determined for the plasma at  $P=33.3$  Pa, 66.6 Pa, and 133.3 Pa and  $V_{\text{pp}}=300$  V are listed in Table I. No contribution to the excitation from  $4^3P$  to  $5^3D$  by atom collisions has been measured, which results from the fact that this excitation energy is 0.334 eV while the atomic kinetic energy at room temperature is only 0.03 eV. On the other hand, in the case of the  $4^3P-4^3D$  transfer the excitation energy is only 0.028 eV.

The electron collision transfer rates  $R_j^{\text{el}}$  are calculated from Eq. (5) and then Eqs. (7) are numerically solved for  $n_e$  and  $T_e$ . In the case of our rf plasma, the Maxwellian EEDF is assumed. This is based on the reports by Godyak and Piejak<sup>3</sup> where only a high energy tail shows deviations from this distribution. High energy electrons, however, play no role in excitation of closely spaced levels as the cross section for this process rapidly decreases with energy. Therefore, the measured  $T_e$  corresponds exclusively to thermal electrons.

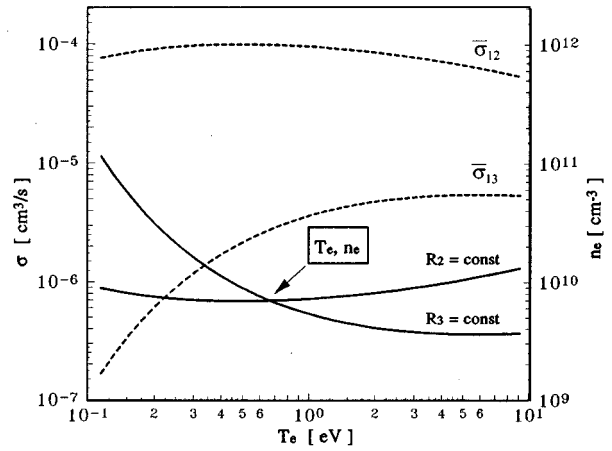


FIG. 3. Electron densities (solid curves) vs electron temperature calculated from experimentally determined electron collision transfer rates  $R_2^{\text{el}}$  and  $R_3^{\text{el}}$  using theoretical values of average electron excitation cross sections (dotted curves). The intersection of two solid curves gives the investigated  $n_e$  and  $T_e$ .

The average electron excitation cross sections are calculated from a semiempirical formula presented in Sobelman.<sup>14</sup> Figure 3 (dashed lines) shows  $\bar{\sigma}$  as a function of electron temperature for the processes discussed in this paper. While  $\bar{\sigma}_{13}$  continuously increases up to about 3 eV,  $\bar{\sigma}_{12}$  is only weakly dependent on  $T_e$  in the same energy range.

The graphic solution of Eq. (7) is shown in Fig. 3 as an intersection of two curves (solid lines). They represent electron densities as a function of electron temperature calculated from Eqs. (7) using experimentally determined electron collision transfer rates  $R_2^{\text{el}}$  and  $R_3^{\text{el}}$ .

For all plasma conditions ( $P=33.3$  Pa through 133.3 Pa and  $V_{\text{pp}}=75$  V through 300 V) the electron temperature is found to be 0.5 eV within the 40% experimental uncertainty, independent on radial and axial positions. Such a large uncertainty arises from the low signal-to-noise ratio for the LCIF signal detected from the  $5^3D$  state. This, however causes only a minor electron density error as one can conclude from Fig. 3.

Figure 4 is a plot of  $n_e$  as a function of the radial position,  $r$ , measured with the LCIF method in the helium discharge at  $V_{\text{pp}}=200$  V and at pressure of 66.7 Pa. The radial position  $r=0$  corresponds to the axis of symmetry of the discharge. The charge density is radially uniform in the majority of the discharge and drops outside the electrode edge. Unlike argon discharges in the GEC reactor,<sup>15</sup> no  $n_e$  peak at the electrode edge has been found.

The axial variation of the electron concentration, under the same discharge conditions as Fig. 4 and for  $r=0$ , is shown in Fig. 5. Axial positions at 0 and 25.4 mm correspond to the powered and grounded electrode, respectively. The charge density exhibits a maximum close to the center of the discharge gap and drops in the direction of both electrodes. This is similar to the axial dependence predicted by various theoretical models of rf glow discharges.<sup>16,17</sup>

Electron densities, determined by the LCIF method in rf helium discharge at 33.3, 66.6, and 133.2 Pa are plotted in

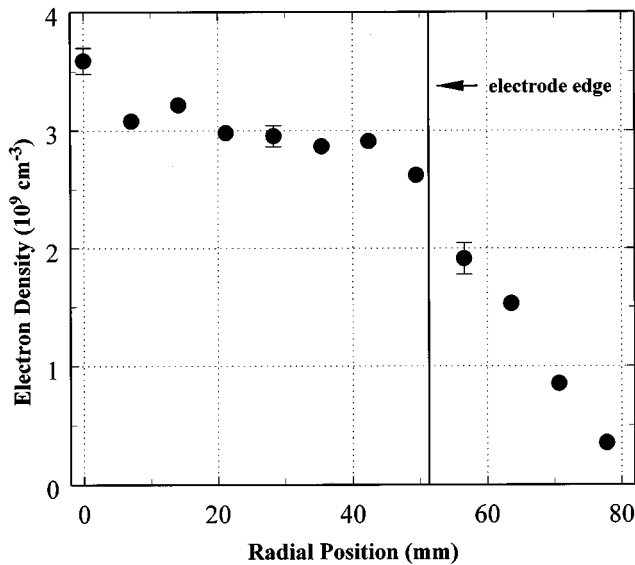


FIG. 4. Radial distribution of electron density determined for  $P=66.6$  Pa,  $V_{pp}=200$  V. Data taken at the center between the electrodes. The error bars represent the standard deviation of five independent measurements of the electron density.

Fig. 6 together with microwave interferometer results from other GEC rf reference cells.<sup>7,18,19</sup> The electron densities are plotted as a function of  $V_{pe}$ , the rf voltage amplitude across the electrodes at the fundamental frequency.  $V_{pe}$  is determined with an equivalent circuit model from the voltage and current wave forms measured at the electrical feed through of the powered electrode.<sup>20</sup> In this way the influence of the stray capacitances, which may vary between cell to cell, can be eliminated. Although all these measurements were made in GEC rf reference cells, none of them were done under identical circumstances.

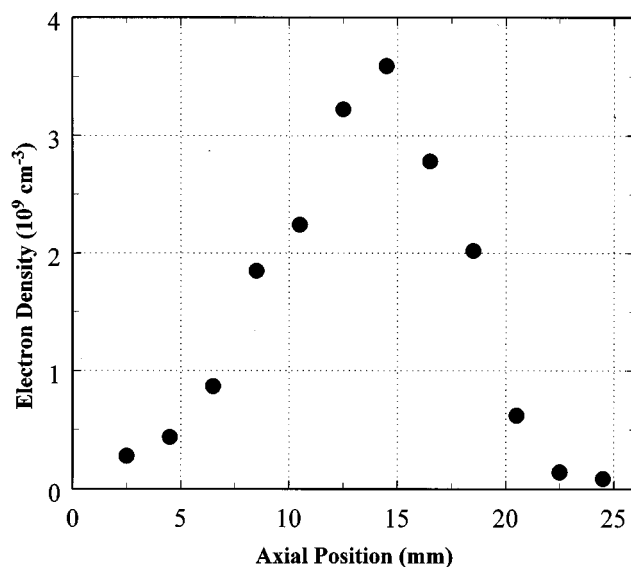


FIG. 5. Axial distribution of electron density determined for  $P=66.6$  Pa,  $V_{pp}=200$  V, radial position,  $r=0$ . The 0 and 25 mm axial positions correspond to the powered and grounded electrode, respectively.

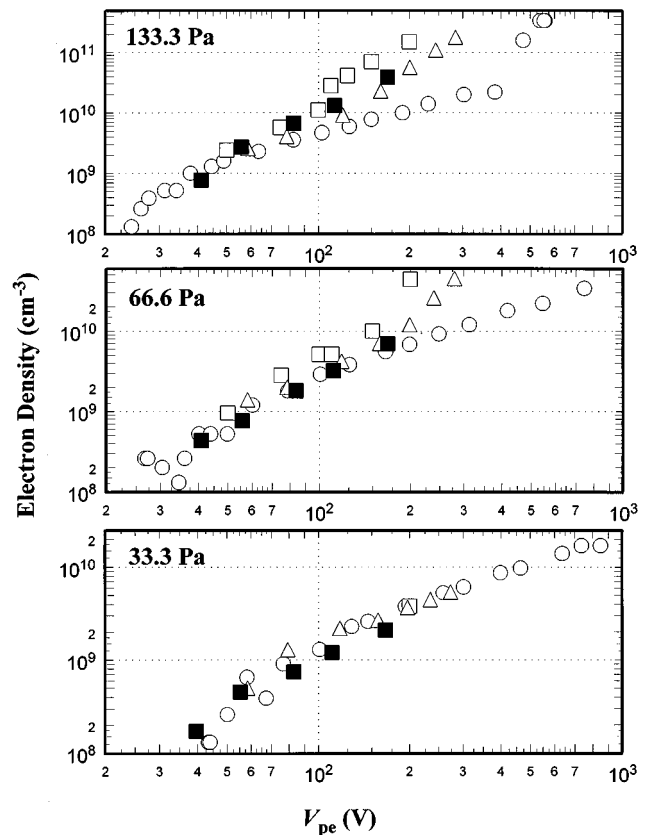


FIG. 6. Electron densities of rf helium discharge as a function of applied voltage (at fundamental frequency). ■, present work, □, Greenberg (see Ref. 7) ○, Overzet (see Ref. 19), △, Bletzinger (see Ref. 18).

The measurements by Greenberg and Hebner were made in a symmetrically powered cell with aluminum electrodes. All the other cells were asymmetrically powered, but Overzet<sup>15</sup> used stainless steel electrodes, Bletzinger<sup>18</sup> used aluminum electrodes, and our measurements were made with an aluminum powered electrode and a stainless steel grounded electrode. In all measurements, except for Overzet, the inferred electron densities scale approximately linearly with applied voltage. While reasonably good agreement between different experiments exists for all applied pressures at lower voltages, the growing discrepancy with increasing pressure and voltage is evident and reaches one order of magnitude in the worst case. For all plasma conditions investigated in our work, very good agreement has been reached with Bletzinger. Both Bletzinger's plasma and our own were made with an aluminum powered electrode. The reason for the discrepancies with two other experiments, we believe is the mechanism by which the discharge is sustained. Application of a steel powered electrode instead of an aluminum electrode would lower the emission of secondary electrons and lead to the transition from an  $\alpha$  mode into a  $\gamma$  mode at higher voltages.<sup>7,21,22</sup> Therefore, Overzet's plasma would be expected to have lower electron concentrations at higher voltages. While Overzet and Bletzinger interferometers filled the entire volume between the electrodes, the Greenberg in-

terferometer was set to fill only the glow space without sheath region so higher electron concentrations can be expected.

## CONCLUSIONS AND REMARKS

The nonintrusive LCIF method was used to measure both the electron concentration and temperature of rf helium discharges in the GEC rf reference reactor. Highly resolved radial and axial profiles of the electron density were determined. The radial profile was uniform over most of the discharge, while the axial profile had a maximum at the center between the electrodes and drops in the direction of both electrodes. The comparison of different experiments shows the growing discrepancy with increasing pressure and voltage. Nevertheless, reasonable agreement of our results with Bletzinger has been achieved, which may indicate that the discrepancies are due mainly to the different materials from which the powered electrodes were made.

The potential application of LCIF to the measurement of electron temperature and density is not restricted to helium. In principle, this technique can be applied to a variety of atomic, ionic, and molecular systems if the laser excitation (one or more photons) from a highly populated ground state or metastable state is possible and if the appropriate electron excitation cross sections are known. The latter is the most serious limitation to the use of LCIF measurements since, unlike many ground or metastable states, the electron excitation cross sections between higher energy excited states are not well known.

To make LCIF results reliable some additional requirements have to be met. (1) Plasma needs to be optically thin at all utilized optical transitions. (2) The contribution of atom and ion collisions to the final state must be taken into account. (3) The states being populated by electron excitation must have average electron excitation cross sections with different electron energy dependence in order to accurately determine  $n_e$  and  $T_e$ .

Therefore, if the theoretical electron excitation cross sections are accurately known and if the above requirements can be met, the LCIF method can provide a nonintrusive, spatially resolved diagnostic of the electron temperature and density in a wide variety of atomic, ionic, or molecular systems.

- <sup>1</sup>N. Hershkovitz, in *Plasma Diagnostics*, edited by O. Aucciello and D. Flamm (Academic, New York, 1989), Vol. 1.
- <sup>2</sup>A. P. Paranjpe, J. P. McVittie, and S. A. Self, *J. Appl. Phys.* **67**, 6718 (1990).
- <sup>3</sup>V. A. Godyak and R. B. Piejak, *J. Appl. Phys.* **68**, 3157 (1990).
- <sup>4</sup>M. J. Goeckner, J. Goree, and T. E. Sheridan, *J. Vac. Sci. Technol. A* **8**, 3920 (1990).
- <sup>5</sup>C. Lai, R. A. Breun, P. W. Sandstrom, A. E. Wendt, N. Hershkovitz, and R. Claude Woods, *J. Vac. Sci. Technol. A* **11**, 1199 (1993).
- <sup>6</sup>L. J. Overzet and M. B. Hopkins, *J. Appl. Phys.* **74**, 4323 (1993).
- <sup>7</sup>K. E. Greenberg and G. A. Hebner, *J. Appl. Phys.* **73**, 8126 (1993).
- <sup>8</sup>B. Dubreuil and P. Prigent, *J. Phys. B* **18**, 4597 (1985).
- <sup>9</sup>K. Tsuchida, S. Miyake, K. Kadota, and J. Fujita, *Plasma Phys.* **25**, 991 (1983).
- <sup>10</sup>E. A. Den Hartog, T. R. O'Brian, and J. E. Lawler, *Phys. Rev. Lett.* **62**, 1500 (1989).
- <sup>11</sup>P. J. Hargis *et al.*, *Rev. Sci. Instrum.* **65**, 140 (1994).
- <sup>12</sup>J. K. Olthoff and K. E. Greenberg, *J. Res. Natl. Inst. Stand. Technol.* **100**, 327 (1995).
- <sup>13</sup>W. L. Wiese, M. W. Smith, and B. M. Glennon, *Atomic Transition Probabilities* (NSRDS-NBS4, 1966), Vol. 1, p. 9.
- <sup>14</sup>I. I. Sobelman, L. A. Vainshtein, and E. A. Yukov, *Excitation of Atoms and Broadening of Spectral Lines* (Springer, New York, 1981), p. 121.
- <sup>15</sup>L. J. Overzet and M. B. Hopkins, *Appl. Phys. Lett.* **63**, 2484 (1993).
- <sup>16</sup>J. P. Boeuf and Ph. Belengeur, in *Nonequilibrium Processes in Partially Ionized Gases*, edited by M. Capitelli and J. N. Bardsley (Plenum, New York, 1991).
- <sup>17</sup>T. J. Sommerer and M. J. Kushner, *J. Appl. Phys.* **71**, 1654 (1992).
- <sup>18</sup>P. Bletzinger and A. Garscaden, Presented at the IEEE Conference on Plasma Science, Williamsburg, VA, 3-5 June 1991 (unpublished).
- <sup>19</sup>L. J. Overzet, *J. Res. Natl. Inst. Stand. Technol.* **100**, 401 (1995).
- <sup>20</sup>M. A. Sobolewski and J. R. Whetstone, *Proc. SPIE* **1803**, 309 (1992).
- <sup>21</sup>V. A. Godyak, R. B. Piejak, and B. M. Alexandrovich, *Plasma Sources Sci. Technol.* **1**, 36 (1992).
- <sup>22</sup>R. Flohr, A. Melzer, and A. Piel, *Plasma Sources Sci. Technol.* **3**, 106 (1994).